Effects of Cu diffusion-doping on structural, optical, and magnetic properties of ZnO nanorod arrays grown by vapor phase transport method

S. Ylmaz, E. McGlynn, E. Bacaksz, . Özcan, D. Byrne et al.

Citation: J. Appl. Phys. **111**, 013903 (2012); doi: 10.1063/1.3673861
View online: http://dx.doi.org/10.1063/1.3673861
View Table of Contents: http://jap.aip.org/resource/1/JAPIAU/v111/i1
Published by the American Institute of Physics.

Effects of Cu diffusion-doping on structural, optical, and magnetic properties of ZnO nanorod arrays grown by vapor phase transport method

S. Yılmaz,[1,2,a)] E. McGlynn,[1] E. Bacaksız,[2] Ş. Özcan,[3] D. Byrne,[1] M. O. Henry,[1] and R. K. Chellappan[4]
[1]*School of Physical Sciences and National Centre for Plasma Science and Technology, Dublin City University, Glasnevin, Dublin 9, Ireland*
[2]*Department of Physics, Faculty of Sciences, Karadeniz Technical University, 61080 Trabzon, Turkey*
[3]*SNTG Laboratory, Physics Engineering Department, Hacettepe University, Beytepe, 06800 Ankara, Turkey*
[4]*School of Physical Sciences and National Centre for Sensor Research, Dublin City University, Glasnevin, Dublin 9, Ireland*

(Received 20 September 2011; accepted 5 December 2011; published online 3 January 2012)

Well-aligned ZnO nanorods were prepared by the vapor phase transport method on Si covered with a ZnO buffer layer. After the nanostructure growth, Cu was doped into the ZnO nanorods by diffusion at three different temperatures and for different times. Undoped and Cu diffusion-doped ZnO samples are highly textured, with the c axis of the wurtzite structure along the growth direction. The incorporation of Cu caused some slight changes in the nanorod alignment, although the wurtzite crystal structure was maintained. X-ray photoelectron spectroscopy measurements revealed that Cu ions were in a divalent state and substituted for the Zn^{2+} ions of the ZnO matrix. Photoluminescence results at 10 K indicate that the incorporation of copper leads to a relative increase of Cu-related structured green band deep level intensity. Magnetic measurements revealed that both undoped and Cu diffusion-doped ZnO samples exhibited room temperature ferromagnetism. It was also found that bound magnetic polarons play an important role in the appearance of room temperature ferromagnetism in Cu diffusion-doped ZnO nanorods. © *2012 American Institute of Physics*. [doi:10.1063/1.3673861]

I. INTRODUCTION

One-dimensional materials including nanowires, nanorods, nanobelts, and nanotubes have drawn much attention due to their importance in basic scientific research and potential technological applications in nanodevices such as nanowire field-effect-transistors, nanolasers, and nanogenerator.[1–3] Among the already known semiconductor nanomaterials, ZnO has attracted increasing interest due to its potential applications in many areas such as field-emission displays, solar cells, and gas sensors.[4] ZnO has also emerged as a promising material for dilute magnetic semiconductors (DMSs).[5] DMS are formed by partial replacement of cations in a nonmagnetic semiconductor by 3 d transition metal ions (e.g., Co, Mn, Fe, Cr, Ni, and Cu) and are currently attractive materials for semiconductor spintronic applications.[6] The field of semiconductor spintronics has the goal of utilizing the spin as well as the charge of the carriers in a new generation of devices such as spin-valve transistors, spin light-emitting diodes, and logic devices.[7–9] To realize these devices, it is necessary to develop semiconducting materials that show ferromagnetism at room temperature. In 2000, Dietl *et al.*[10] predicted theoretically that Mn-doped ZnO and GaN would be ferromagnetic at room temperature and would, therefore, be suitable for applications in spintronics. Following this direction, using *ab-initio* calculations based on the local density approximation, Sato and Katayama-Yoshida[11] theoretically demonstrated that V-, Fe-, Co-, Ni-, and Cr-doped ZnO should show ferromagnetic ordering at and above room temperature. After these theoretical studies, Ueda *et al.*[12] experimentally reported ferromagnetic behavior with a Curie temperature higher than room temperature for Co-doped ZnO films grown by pulsed laser deposition, however Jin *et al.*[13] observed no indication of ferromagnetism in films grown on sapphire (0001) by laser molecular beam epitaxy. Early studies explained ferromagnetism in ZnO in terms of a free carrier mediated mechanism resulting from ferromagnetic behavior in oxide based DMS.[11] However, more recent studies proposed that defects like oxygen vacancies are giving rise to ferromagnetic ordering.[14] These results are indicative of the broader state of affairs with regard to ZnO, i.e., that there is no consensus on ferromagnetic behavior and its origin for ZnO-based materials.

Recently, there has been a lot of interest in studying transition metal-doped ZnO nanostructures.[15–17] Among these reports, Cu-doped ZnO studies have aroused a lot of interest because the substitution of Cu at the sites of Zn atoms with appropriate doping content supports a ferromagnetic ground state which was proposed by several first principles calculations.[18–20] These theoretical predictions were later supported by experimental observations of room temperature ferromagnetism in Cu-doped ZnO thin films.[21–23] However, there are few reports on one-dimensional Cu-doped ZnO nanostructures, especially well-aligned nanorod arrays.[15,24]

There are various methods to fabricate one-dimensional transition metal-doped ZnO materials. These techniques include chemical vapor deposition,[25] hydrothermal method,[26] thermal evaporation,[27] ion implantation,[28] and vapor phase

a)Author to whom correspondence should be addressed. Electronic mail: s_yilmaz@ktu.edu.tr.

transport method (VPT).[29] Among these methods, VPT method is widely used because of relatively simple apparatus requirements and has been employed to fabricate various nanostructures of ZnO.[30,31] Furthermore, there is much less research on the use of VPT method for the growth of one-dimensional transition metal-doped ZnO materials in the literature and it is our intention to undertake a novel and necessary study of the use and potential of this growth method to grow ZnO-based DMS. In this communication, we present data on well-aligned ZnO nanorod arrays synthesized via VPT on ZnO buffer layer coated Si substrates and specifically we study the effects of different annealing temperatures and times on Cu diffusion-doped samples using x-ray diffraction (XRD), scanning electron microscopy (SEM), x-ray photoelectron spectroscopy (XPS), photoluminescence (PL), and magnetic measurements. We discuss the relationship between the optical and magnetic properties with a view to explaining the origin of observed room temperature ferromagnetism in our Cu diffusion-doped ZnO nanorod samples.

II. EXPERIMENTAL DETAILS

Well aligned ZnO nanorods were grown on silicon substrates using a three step approach consisting of an initial seeding of substrates and followed by a chemical bath deposition (CBD) and finally VPT nanorod growth. Full details of the growth method may be found in Ref. 32.

n-type Si (100) wafers (thickness $508 \pm 20\,\mu$m, resistivity 5–9 Ω cm) were cut into 1×1.5 cm^2 pieces as substrates, cleaned ultrasonically in sequence with acetone, ethanol, and then blown dry with a nitrogen flow. To grow the ZnO seed layer, zinc acetate dihydrate ($Zn(OOCCH_3)_2{\cdot}2H_2O$) was dissolved in the absolute ethanol with concentration of 5 mM and this solution was coated onto Si wafers by drop coating with a volume per area of 3.5 μL/cm^2. The substrates were rinsed with fresh ethanol after drop coating after 20 s and then dried with a nitrogen stream. This procedure was repeated five times for each sample and then the samples were annealed at 350 °C for 30 min in ambient air to produce the initial textured ZnO seed layer which provides nucleation sites for subsequent steps and also provides good alignment to the ZnO nanorods to be grown by the CBD method, as described in Refs. 32 and 33.

In the CBD process, 25 mM zinc nitrate hexahydrate ($Zn(NO_3)_2.6H_2O$) was dissolved in deionized water (40 ml) and 25 mM hexamethylenetetramine ($C_6H_{12}N_4$) was added to the solution to induce the formation of ZnO nanorods.[34] ZnO seeded substrates were immersed vertically into the aqueous solution and heated at a constant temperature of 80 °C using water baths for 40 min, with stirring. After deposition, samples were taken from the solution, ultrasonically cleaned with deionized water for 5 min to remove white loosely adherent powder precipitates, rinsed with ethanol, and dried with nitrogen.

For the VPT growth stage, 0.06 g of ZnO and graphite powders were thoroughly mixed together and placed in the middle of an alumina boat. Substrates which were covered ZnO buffer layers (seed layer plus CBD) were placed directly above the source material with the growth surface facing the powder. The boat was loaded in the central part of a tube furnace. The growth was carried out at 925 °C with a 90 sccm flow of argon for 1 h. The furnace was then cooled down to room temperature and the samples were taken out.

Cu metal with purity of 99.98 at. % was evaporated on the vertically aligned ZnO nanorods by e-beam evaporation (Leybold Univex 350). The system pressure during deposition was $\sim 6 \times 10^{-6}$ Torr. The amount of copper deposited onto ZnO nanorods was controlled by a quartz crystal thickness monitor (Inficon XTM/2) and equivalent thickness of the Cu layer was ~5 nm. After the Cu deposition, the samples were annealed in a quartz tube at various temperatures ranging from 500 °C to 700 °C for 8 h and a fixed temperatures of 700 °C for different times ranging from 8 h to 24 h in a vacuum of $\sim 10^{-2}$ Torr.

The crystal structure of the samples was investigated using a Bruker AXS D8 advance texture diffractometer with CuK_α radiation, operated at a voltage of 40 kV, and a current of 40 mA, over the range $2\theta = 20°$–$60°$ with a step of 0.01° at room temperature. The crystal quality was further studied by x-ray rocking curve (XRC) measurements of the ZnO (002) reflection. The surface morphology and bulk composition were studied with a Zeiss EVOLS 15 SEM equipped with energy dispersive x-ray spectroscopy (EDS). An acceleration voltage of 20 kV was used in all cases for these studies. The chemical composition and bonding at the surface (sampling depth ~5 nm) were characterized by using XPS with Al Kα radiation (1486.6 eV). The kinetic energy of the photo emitted electrons from the surface was measured in an electron energy analyzer, operated in constant pass energy mode under ultra high vacuum ($\sim 10^{-10}$ mbar). Due to charging effects, the C 1 s photoelectron peak at 285.0 eV was consistently used as a reference for the charge-correction of binding energies of core level peaks. PL measurements were performed at 10 K, using a SPEX 1704 monochromator, with a closed cycle cryostat (Janis SHI-950-5). PL spectra were excited with the 325 nm line of a He–Cd laser operating at 200 mW. Magnetization measurements of the samples as a function of magnetic field and temperature were carried out using a quantum design physical property measurement system (PPMS) system with a vibrating sample magnetometer module.

III. RESULTS AND DISCUSSION

Figs. 1(a)–1(d) shows the powder 2θ-ω XRD patterns of undoped and Cu diffused ZnO nanorods annealed at a constant temperature of 700 °C for 8 h, 16 h, and 24 h in vacuum atmosphere, respectively. The only peak related to ZnO is the (002) peak and these XRD results suggest that all the samples have the hexagonal wurtzite structure with a highly c-axis preferred orientation perpendicular to the substrate, which is consistent with the SEM results shown later. No traces of copper and its oxides such as CuO, Cu_2O were detected in our samples within the detection limit of the XRD measurements. The ZnO (002) reflection peak of undoped ZnO nanorods is located at 34.43° which corresponds to a c-lattice parameter value of 5.21 Å, consistent with the value for bulk material within the accuracy of our experimental system.[35] Compared with the undoped sample, the c-lattice constant values of ZnO:Cu samples have not changed significantly, probably due to the very similar ionic radii of Zn^{2+} (0.74 Å) and Cu^{2+}

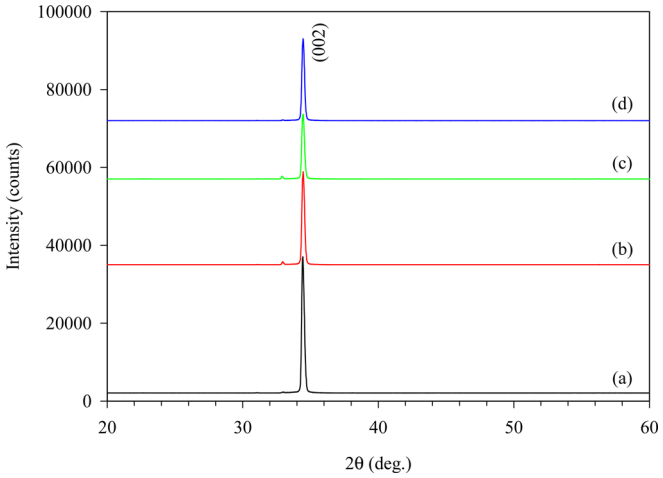

FIG. 1. (Color online) XRD patterns of undoped ZnO (a), and Cu diffusion-doped ZnO nanorods annealed at 700 °C for 8 h (b), 16 h (c), and 24 h (d).

(0.73 Å). The weak peak at ~33° is due to the nominally forbidden Si (002) reflection which is allowed by double diffraction effects.[36]

To further investigate the crystallinity and alignment of the one-dimensional ZnO nanorods, XRC measurements were carried out. Figs. 2(a)–2(d) presents the XRC data for the ZnO (002) diffraction peaks obtained from the same samples shown in Fig. 1 (and in the same order). The full width at half-maximum (FWHM) value of the undoped ZnO sample is 3.36°, which indicates excellent alignment of the nanorods perpendicular to the substrate surface. A very similar value of XRC FWHM was reported by Wang *et al.*[37] for Cu-doped ZnO films synthesized with magnetron sputtering. On the other hand, Yanmei *et al.*[38] found a larger FWHM value of 10.4° for undoped ZnO in hydrothermal grown Ni:ZnO nanorods. After Cu evaporation and subsequent annealing and diffusion, the intensity of the ZnO (002) peak compared to the undoped ZnO firstly decreases slightly and then increases slightly for the sample annealed at 700 °C for 24 h. This change in (002) intensity is likely to be related to changes in the FWHM values which firstly increases to 5.08°

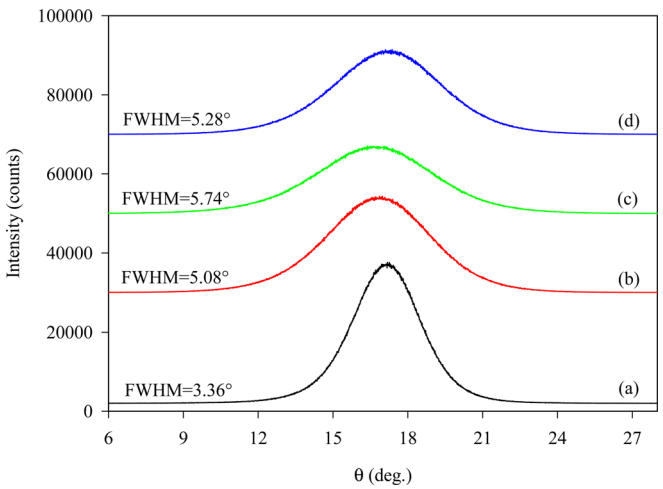

FIG. 2. (Color online) The Rocking curves of undoped ZnO (a), and Cu diffusion-doped ZnO nanorods annealed at 700 °C for 8 h (b), 16 h (c), and 24 h (d).

and 5.74° for the samples annealed 700 °C for 8 and 16 h, respectively, and then decreases to 5.28° (Ref. 39).

The surface morphology of nanorods on ZnO buffer layer coated Si substrates was investigated by SEM. Figs. 3(a)–3(d) shows typical SEM images of ZnO nanorods for the sample diffusion-doped with Cu and annealed at 700 °C for 16 h. Fig. 3(a) and 3(b) illustrate top view and 45° tilted view images of the ZnO:Cu nanorod arrays, respectively, implying that ZnO:Cu samples grew uniformly over a large area. The magnified image of the top view is presented in the inset of Fig. 3(a), showing that ZnO:Cu nanorods have a well-defined hexagonal prism shape with a diameter of ~100 nm. Figs. 3(c) and 3(d) display a 45° tilted view image obtained from the edge of the sample and cross-section image of ZnO:Cu nanorod arrays, respectively, showing that all the ZnO nanorods grow predominantly vertical to the ZnO buffer layer coated Si substrates, in support of XRD and XRC data, and that almost all nanorods have similar lengths, typically up to 4.0 μm long.

Chemical composition and elemental homogeneity of the samples were determined by EDS. Fig. 4(a) shows the SEM image obtained from ZnO:Cu nanorod sample annealed at 700 °C for 16 h. Figs. 4(b)–4(d) indicates EDS mapping of Zn, O, and Cu elements, respectively. As can be seen in Figs. 4(b)–4(d), Zn, O, and Cu elements indicate a uniform distribution in the ZnO:Cu sample annealed at 700 °C for 16 h. In addition, it was found that the atomic ratio of Cu/Zn+O for ZnO:Cu annealed at 600 °C for 8 h was ~0.64 at. %, however, the atomic ratios of Cu/Zn+O of all the other ZnO:Cu samples had the same value of ~1 at. %.

The incorporation of Cu ions into the ZnO lattice and their valence states were characterized by XPS measurements. Fig. 5(a) shows the full-range XPS survey spectrum for undoped ZnO and ZnO:Cu nanorods annealed at 700 °C for 24 h and only peaks corresponding to Zn, C, O, and Cu are identified. Fig. 5(b) illustrates Cu 2 p core-level XPS spectra of ZnO:Cu sample annealed at 700 °C for 24 h in vacuum. As can be seen from Fig. 5(b), the 2 p level is split into a doublet with an energy separation due to the spin–orbit interaction.[40] Cu 2p3/2 and 2p1/2 core levels of the sample were fitted with Gaussian functions and centered at 933.7 and 953.5 eV, respectively, implying that Cu is in a divalent valence state, which is good agreement with the other studies in the literature.[41,42] Furthermore, a satellite peak is observed at binding energies in the range of 940-945 eV. CuO (Cu^{2+}) differs from metallic copper (Cu^0) and Cu_2O (Cu^{1+}) because Cu^{2+} is known to have Cu 2 p satellite peaks at higher binding energy associated with the existence of Cu 3 d hole states (Cu 3 d^9). However, Cu^{1+} and Cu^0 do not exhibit any satellite peaks since the 3 d band of Cu_2O is filled (Cu 3 d^{10}) and the 4 s band is unoccupied.[43,44] Thus, based on all the discussions above, we can conclude that Cu is in a divalent valence state.

In order to investigate the influence of Cu diffusion doping on optical emission and defect formation, PL spectra of all the samples were measured at 10 K. Figs. 6(a)–6(f) shows PL spectra of undoped and Cu diffusion-doped ZnO nanorods annealed at 500 °C, 600 °C, and 700 °C for 8 h and at 700 °C for 16 h and 24 h, respectively (all spectra normalized to the near band edge (NBE) peak emission). The dominant UV peak seen in all the samples is located at ~3.367 eV and

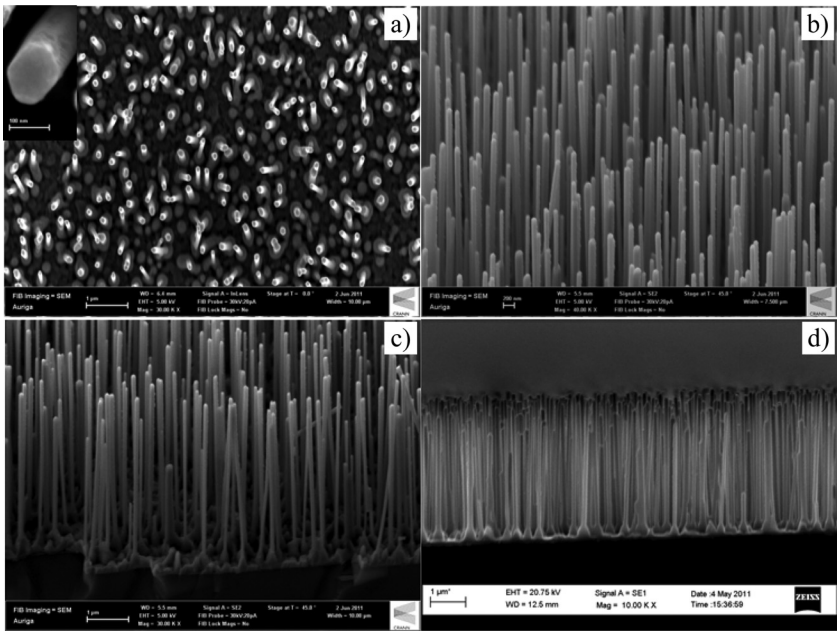

FIG. 3. SEM images of (a) Top view, (b) 45° tilted view, (c) 45° tilted view obtained from edge of sample, and (d) cross-section of ZnO:Cu nanorods annealed at 700 °C for 16 h.

is ascribed to the NBE emission due to excitons bound to donors (D^0X, members of the so-called I line series).[45] The energies of these peaks are identical within about 4 meV for all samples, indicating that the dominant donor bound exciton emission energy is not significantly affected by the Cu incorporation. This D^0X emission is observed at a constant energy below the band gap and thus indicates that the band gaps at low temperatures in all samples are identical. The inset of the Fig. 6 shows PL data of ZnO:Cu nanorod arrays annealed at 500 °C for 8 h measured at 10 K in the range of 366-371 nm, scanned with a step size of 0.04 nm. As can be seen from the inset, dominant lines located at energies 3.357 eV and 3.361 eV result from the neutral donor bound excitons of I_9 and I_6, which are ascribed to Al and In donors, respectively. The content of In may come from source of powder used in our VPT system. The origin of Al contamination may be due to both source of powder and alumina boat used to evaporate the powder mixture. Various other higher energy bound exciton lines are seen due to other impurities and also to excited states of neutral donor bound excitons and ionized donor bound excitons and the free exciton emission positioned at >3.375 eV can be seen in the higher photon energy region of the spectrum.[45]

The deep level visible emission (DLE) region which is in the range of 430-650 nm is usually attributed (depending on the details of its shape and temperature dependence) to intrinsic defects such as zinc vacancy (V_{Zn}), interstitial zinc (Zn_i), oxygen vacancy (V_o) and oxygen interstitial (O_i) (for the case of the unstructured green band), as well as extrinsic impurities, such as substitutional Cu (for the structured green band).[46,47] The structured green luminescence band was clearly observed in our samples. The energy spacing between two adjacent lines in the structure is almost 72 meV and can be attributed to the LO phonon replicas.[48] As illustrated in Fig. 6, Cu-diffused ZnO nanorods display this structured visible luminescence band which increases gradually in relative intensity with both annealing temperature and time indicating that Cu atoms have substituted into ZnO lattice sites.[49] There is likely to also be

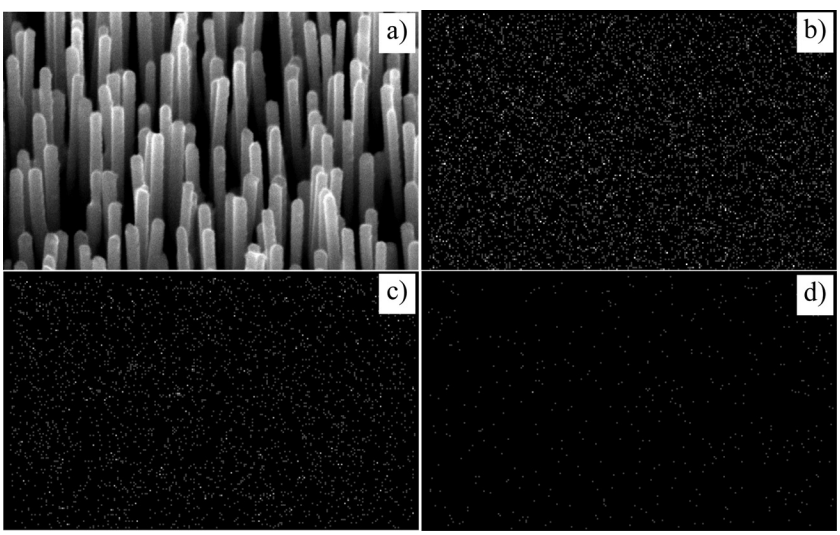

FIG. 4. (a) A SEM image and EDS mapping of (b) Zn, (c) O, and (d) Cu elements of ZnO:Cu nanorod sample annealed at 700 °C for 16 h.

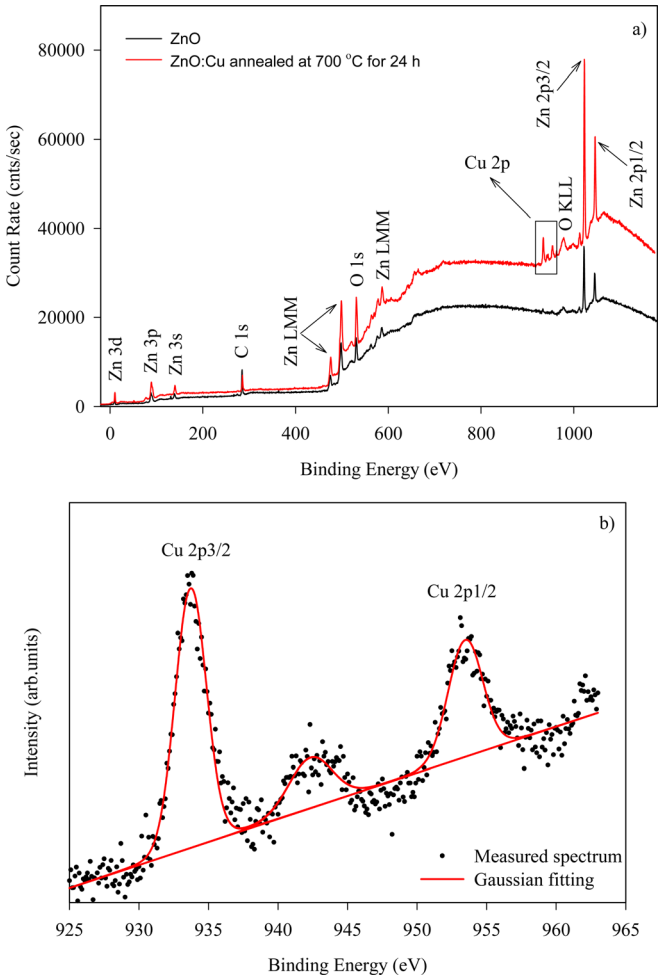

FIG. 5. (Color online) (a) XPS survey spectra of undoped and Cu diffusion-doped ZnO nanorod array annealed at 700 °C for 24 h, (b) shows binding energy spectrum of Cu 2p and Gaussian fitting.

simultaneous creation of point defects due to the vacuum annealing (to create V_o) and/or effects of Cu incorporation into Zn sites and hence there may be some complexing of Cu with native defects.[50] In principle, the creation of V_o defects should also lead to an increase of the unstructured green band but this is probably masked in our samples by the strong Cu-related structured green band in the same spectral region.

The electrical conductivity properties of the film are also of relevance to analyses of the present type. The present samples are in the form of nanorods and thus do not form a continuous conducting film (noting also that the underlying buffer layer is quite thin and with a small grain size and thus will not show significant conductivity). The nanorod morphology means that measuring the conducting properties of individual nanorods is quite challenging. However, the presence of a range of I-line defects associated with donor bound excitons in the low temperature PL spectra of the samples indicates that these samples display background n-type conductivity in the nominally undoped condition, in line with the overwhelming majority of literature reports for nominally undoped ZnO material. Nominally, undoped ZnO nanorod samples are known from the literature to have carrier densities and mobilities of the order of 10^{17} cm^{-3} and 10 cm^2 V^{-1} s^{-1}, respectively,[51] and we feel that our nominally undoped samples, of similar crystalline quality

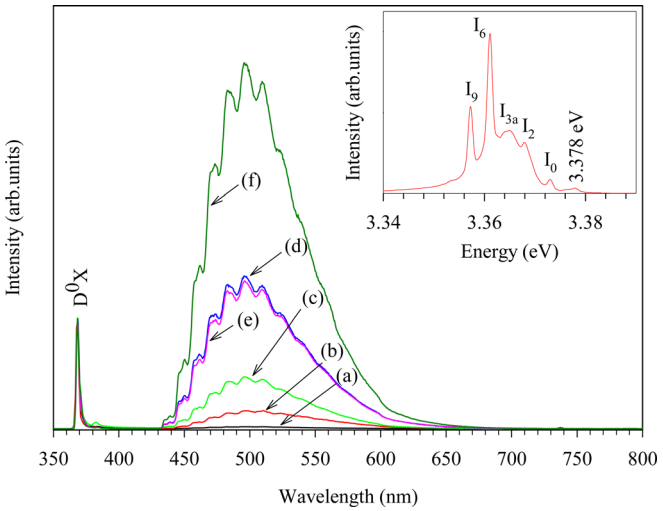

FIG. 6. (Color online) Low temperature PL spectra of undoped ZnO (a) and Cu diffusion-doped ZnO nanorods annealed at 500 °C for 8 h (b), 600 °C for 8 h (c), 700 °C for 8 h (d), 700 °C for 16 h (e), and 700 °C for 24 h (f).

and grown at similar temperatures, would likely display similar electrical properties. Doping with Cu, which can act as a deep acceptor,[49] is likely to compensate some of the donors and lead to a reduction in free electron density, and most likely a reduction in mobility also due to increased defect scattering.

There is much evidence to suggest that ferromagnetism in transition-metal (TM) doped ZnO is unambiguously correlated with defects, which depend on the substrate temperature and oxygen pressure used during film deposition;[6,52] the charge carriers are by products of these defects. Ney *et al.*[53] have demonstrated that highly perfect Co-doped epitaxial films, for example, are purely paramagnetic, with cobalt occupying zinc sites and no sign of anything other than weak antiferromagnetic Co-O-Co nearest-neighbor superexchange. Droubay *et al.*[54] show that Mn-doped epitaxial films are paramagnetic, with Mn substituting for Zn, and no moments on either oxygen or zinc. Barla *et al.*[55] showed that the cobalt in ferromagnetic Co-doped ZnO films was paramagnetic, and there was no moment on the zinc. A study by Tietze *et al.*[56] who investigated 5 at. % Co-doped films produced by periodic lattice distortion (PLD) which exhibited a moment of $\approx 1\ \mu_B$/Co, corresponding to a magnetization of ≈ 20 kAm^{-1} came to a remarkable conclusion; extensive XMCD (x-ray magnetic circular dichroism) measurements on the Co and O edges with a very good signal/noise ratio showed only the signatures of paramagnetic cobalt and oxygen. There is no sign of element-specific ferromagnetism. By a process of elimination, only oxygen vacancies remained as the possible intrinsic source of the ferromagnetism observed in the ZnO films.

Magnetization curves were measured for all samples at 300 K in the SQUID (superconducting quantum interference device) magnetometer. Data were corrected for the diamagnetic contribution of the Si substrate, which is determined from the high-field linear part of M-H loops. Fig. 7 shows the room temperature magnetization undoped and Cu diffusion-doped ZnO nanorods annealed at 500 °C, 600 °C, and 700 °C for 8 h in vacuum. It can be noted that all the samples exhibit ferromagnetic behavior at room temperature; however Cu diffusion-doped ZnO samples have higher magnetic moment

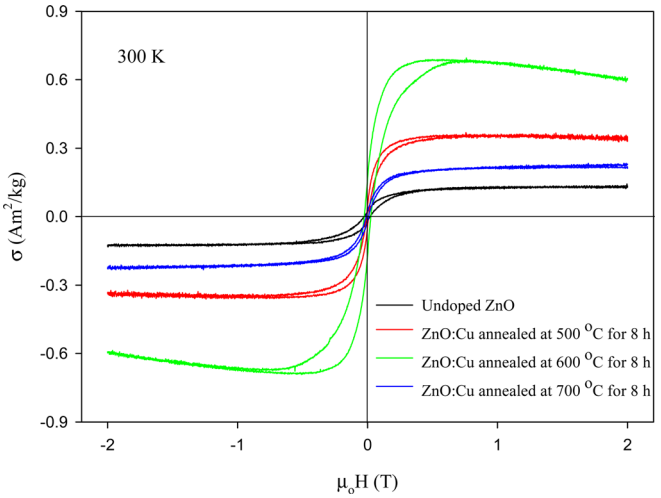

FIG. 7. (Color online) Room temperature M-H curves of undoped ZnO, Cu diffusion-doped ZnO nanorods annealed at 500 °C, 600 °C, and 700 °C for 8 h.

values compared to the pure ZnO one. Similar behaviour was obtained by Kumar *et al.*[57] for Cu-doped ZnO samples. The origin of the ferromagnetism in undoped ZnO is probably due to defects, based on the previous studies mentioned above, suggesting that the magnetic moment does not originate from *d* electrons but rather from localized holes in p-bands carrying a magnetic moment.[58] After annealing the ZnO:Cu nanorods at 500 °C in vacuum, it was found to be the values of saturation magnetization (M_s) and coercive field (H_c) of 0.19 μ_B/Cu and 8 mT, respectively. When the annealing temperature increases from 500 °C to 600 °C, the saturation magnetization of the sample is enhanced significantly and reaches a maximum value of 1.39 μ_B/Cu for the sample annealed at 600 °C. This enhancement may be related to the atomic ratio of Cu/Zn+O, determined from the EDS, because for ZnO:Cu annealed at 600 °C, this ratio is lower than that of the others and has the value of 0.64 at. %, which indicates that Cu solubility in our ZnO nanorods is below 1 at. %.[59] According to the literature, similar trend was observed by Cho *et al.*[60] that showed that magnetization of ZnO:Cu films increases with increasing Cu concentration up to 1 at. % followed by a decrease in ferromagnetic behaviour for Cu content above 1 at. %. Additionally, Sudakar *et al.*[22] found that ZnO films with Cu concentration of $x < 1$ at. % grown by reactive magnetron co-sputtering method on c-cut Al_2O_3 substrates exhibited very clear ferromagnetic behavior with a large M_s value of 1.6 μ_B/Cu, however, for the samples with $x > 1$ at. %, saturation magnetization decreased drastically to 0.4 μ_B/Cu at 2 at. % and 0.1 μ_B/Cu for 6 at. % Cu contents. Samanta *et al.*[61] also produced Cu-doped ZnO thin films with the pulsed laser deposition technique on (0001) oriented sapphire substrates and observed a maximum M_s value of 0.76 μ_B/Cu for 3 at. % Cu-doped ZnO samples at 300 K, however, the saturation magnetization decreased with the further increase of copper concentration. On the other hand, higher annealing temperatures significantly decrease the value of room temperature saturation magnetization and it reaches to 0.31 μ_B/Cu value. One of the reasons for the decrease in magnetization at high temperature may be attributed to movement and annihilation or complexing of zinc interstitial atoms. The number of Zn_i defects decreases at high temperature, which in turn could lead to the decrease in saturation magnetization.[62]

It was proposed that oxygen vacancies and zinc interstitials can cause a marked change in the band structure of host semiconductors and make an important contribution to the ferromagnetism.[63] The formation of bound magnetic polarons (BMPs), which include electrons locally trapped by oxygen vacancy or zinc interstitial, with the trapped electron occupying an orbital overlapping with the d shells of TM neighbors, has also been suggested to explain the origin of ferromagnetism.[64] In addition to these theoretical studies, several experimental groups have reported that the intrinsic defects play crucial roles in the ferromagnetism of TM-doped ZnO. For example, Hsu *et al.*[65] have performed x-ray near edge spectroscopy on Co-doped ZnO films and shown that the enhancement in ferromagnetism is directly related to an increase in oxygen vacancies. Liu *et al.*[66] indicated that point defects such as Zn_i or V_{Zn} are responsible for ferromagnetism in Cr:ZnO samples. Furthermore, Liu *et al.*[67] suggested that two key factors lead to the appearance of ferromagnetism in TM-doped ZnO nanocrystals: one is the increase of the number of defects and oxygen vacancies and the other is the exchange interactions between the TM ions and the O ion spin moment.

The observed ferromagnetism of our Cu diffusion-doped ZnO samples could originate from a number of possible sources. Metallic Cu is diamagnetic and cannot contribute to the observed ferromagnetism. There is no contribution to magnetization from binary copper oxide CuO, which is an antiferromagnetic phase with a Neel temperature of 230 K (Ref. 68) and diamagnetic cupric oxide Cu_2O.[69] In addition, there is no signature metallic Cu or CuO related bases in either XRD or XPS measurements. The room temperature ferromagnetism in our Cu:ZnO samples is intrinsic and probably results from the magnetic exchange interaction between oxygen vacancies and Cu^{2+} ions which aligns all the Cu^{2+} ions around the oxygen vacancies, forming BMPs.[70,71]

IV. CONCLUSIONS

Based on the structural, optical, and magnetic measurements of our samples the following main points emerge: (1) all the samples exhibit hexagonal structure with a strong (002) preferred orientation normal to the substrate; (2) surface morphology analysis has revealed that the ZnO:Cu sample has a well-aligned hexagonal nanorod morphology; (3) XPS results showed the incorporation of Cu^{2+} into Zn sites in the ZnO host lattice; (4) compared to the undoped ZnO, the number of Cu-related optically active deep level defects increased for Cu diffusion-doped ZnO nanorod samples; (5) Cu diffusion-doped ZnO nanorod samples displayed ferromagnetic loops clearly at room temperature and the origin of the observed room temperature ferromagnetism is probably due to interactions between substitutional Cu_{Zn} in a divalent charge with other (intrinsic) point defects, most likely oxygen vacancies, in the crystal.

ACKNOWLEDGMENTS

The corresponding author (S.Y.) gratefully acknowledges the support of the Council of Turkish Higher

Education in the form of a fellowship to support extended visits to foreign institutions.

[1]M. S. Arnold, P. Avouris, Z. W. Pan, and Z. L. Wang, J. Phys. Chem. B **107**, 659 (2003).
[2]M. H. Huang, S. Mao, H. Feick, H. Yan, Y. Wu, H. Kind, E. Weber, R. Russo, and P. Yang, Science **292**, 1897 (2001).
[3]X. Wang, J. Song, J. Liu, and Z. L. Wang, Science **316**, 102 (2007).
[4]C. H. Liu, J. A. Zapien, Y. Yao, X. M. Meng, C. S. Lee, S. S. Fan, Y. Lifshitz, and S. T. Lee, Adv. Mater. **15**, 838 (2003).
[5]J.-J. Wu, S.-C. Liu, and M.-H. Yang, Appl. Phys. Lett. **90**, 062504 (2007).
[6]F. Pan, C. Song, X. J. Liu, Y. C. Yang, and F. Zeng, Mater. Sci. Eng. R **62**, 1 (2008).
[7]J. K. Furdyna, J. Appl. Phys. **64**, R29 (1988).
[8]S. J. Pearton, W. H. Heo, M. Ivill, D. P. Norton, and T. Steiner, Semicond. Sci. Technol. **19**, R59 (2004).
[9]Y. X. Wang, H. Liu, Z. Q. Li, X. X. Zhang, R. K. Zheng, and S. P. Ringer, Appl. Phys. Lett. **89**, 042511 (2006).
[10]T. Dietl, H. Ohno, F. Matsukura, J. Cibert, and D. Ferrand, Science **287**, 1019 (2000).
[11]K. Sato and H. Katayama-Yoshida, Jpn. J. Appl. Phys., Part 2 **39**, L555 (2000).
[12]K. Ueda, H. Tabata, and T. Kawai, Appl. Phys. Lett. **79**, 988 (2001).
[13]Z. Jin, T. Fukumura, M. Kawasaki, K. Ando, H. Saito, T. Sekiguchi, Y. Z. Yoo, M. Murakami, Y. Matsumoto, T. Hasegawa, and H. Koinuma, Appl. Phys. Lett. **78**, 3824 (2001).
[14]J. M. D. Coey, A. P. Douvalis, C. B. Fitzgerald, and M. Venkatesan, Appl. Phys. Lett. **84**, 1332 (2004).
[15]G. Z. Xing, J. B. Yi, J. G. Tao, T. Liu, L. M. Wong, Z. Zhang, G. P. Li, S. J. Wang, J. Ding, T. C. Sum, C. H. A. Huan, and T. Wu, Adv. Mater. **20**, 3521 (2008).
[16]A. Wang, B. Zhang, X. Wang, N. Yao, Z. Gao, Y. Ma, L. Zhang, and H. Ma, J. Phys. D: Appl. Phys. **41**, 215308 (2008).
[17]T.-L. Phan, S. C. Yu, R. Vincent, H. M. Bui, T. D. Thanh, V. D. Lam, and Y. P. Lee, J. Appl. Phys. **108**, 044910 (2010).
[18]D. B. Buchholz, R. P. H. Chang, J. H. Song, and J. B. Ketterson, Appl. Phys. Lett. **87**, 082504 (2005).
[19]L. H. Ye, A. J. Freeman, and B. Delley, Phys. Rev. B **73**, 33203 (2006).
[20]L. M. Huang, A. L. Rosa, and R. Ahuja, Phys. Rev. B **74**, 75206 (2006).
[21]D. Chakraborti, J. Narayan, and J. T. Prater, Appl. Phys. Lett. **90**, 062504 (2007).
[22]C. Sudakar, J. S. Thakur, G. Lawes, R. Naik, and V. M. Naik, Phys. Rev. B **75**, 054423 (2007).
[23]Q. Y. Xu, H. Schmidt, S. Q. Zhou, K. Potzger, M. Helm, H. Hochmuth, M. Lorenz, A. Setzer, P. Esquinazi, C. Meinecke, and M. Grundmann, Appl. Phys. Lett. **92**, 082508 (2008).
[24]T. S. Herng, S. P. Lau, S. F. Yu, H. Y. Yang, L. Wang, M. Tanemura, and J. S. Chen, Appl. Phys. Lett. **90**, 032509 (2007).
[25]J. J. Liu, M. H. Yu, and W. L. Zhou, J. Appl. Phys. **99**, 08M119 (2006).
[26]Y. Zuo, S. Ge, Z. Chen, L. Zhang, X. Zhou, and S. Yan, J. Alloy Compd. **470**, 47 (2009).
[27]K.-H. Zheng, Z. Liu, J. Liu, L.-J. Hu, D.-W. Wang, C.-Y. Chen, and L.-F. Sun, Chin. Phys. B **19**, 026101 (2010).
[28]L.W. Yang, W. L. Wu, T. Qiu, G. G. Siu, and P. K. Chu, J. Appl. Phys. **99**, 074303 (2006).
[29]Y. Q. Chang, D. B. Wang, X. H. Luo, X. Y. Xu, X. H. Chen, L. Li, C. P. Chen, R. M. Wang, J. Xu, and D. P. Yu, Appl. Phys. Lett. **83**, 4020 (2003).
[30]C. X. Xu, X. W. Sun, and B. J. Chen, Appl. Phys. Lett. **84**, 1540 (2004).
[31]M. Biswas, E. McGlynn, M. O. Henry, M. McCann, and A. Rafferty, J. Appl. Phys. **105**, 094306 (2009).
[32]D. Byrne, E. McGlynn, K. Kumar, M. Biswas, M. O. Henry, and G. Hughes, Cryst. Growth Des. **10**, 2400 (2010).
[33]L. E. Greene, M. Law, D. H. Tan, M. Montano, J. Goldberger, G. Somorjai, and P. Yang, Nano Lett. **5**, 1231 (2005).
[34]L. L. Yang, Q. X. Zhao, and M. Willander, J. Alloy Compd. **469**, 623 (2009).
[35]Ü. Özgür, Y. I. Alivov, C. Liu, A. Teke, M. A. Reshchikov, S. Doğan, V. Avrutin, S.-J. Cho, and H. Morkoç, J. Appl. Phys. **98**, 041301 (2005).
[36]B.-H. Hwang, J. Phys. D: Appl. Phys. **34**, 2469 (2001).
[37]X. B. Wang, C. Song, K. W. Geng, F. Zeng, and F. Pan, Appl. Surf. Sci. **253**, 6905 (2007).
[38]L. Yanmei, W. Tao, S. Xia, F. Qingqing, L. Qingrong, S. Xueping, and S. Zaoqi, Appl. Surf. Sci. **257**, 6540 (2011).
[39]E. McCarthy, R. T. R. Kumar, B. Doggett, S. Chakrabarti, R. J. O'Haire, S. B. Newcomb, J.-P. Mosnier, M. O. Henry, and E. McGlynn, J. Phys. D: Appl. Phys. **44**, 375401 (2011).
[40]Y. Y. Peter and M. Cardona, *Fundamentals of Semiconductors: Physics and Material Properties* (Springer, Berlin, 2001).
[41]X. Wang, J. B. Xu, W. Y. Cheung, J. An, and N. Ke, Appl. Phys. Lett. **90**, 212502 (2007).
[42]D. Chakraborti, G. R. Trichy, J. T. Prater, and J. Narayan, J. Phys. D: Appl. Phys. **40**, 7606 (2007).
[43]J.-B. Lee, H.-J. Lee, S.-H. Seo, and J.-S. Park, Thin Solid Films **398**, 641 (2001).
[44]J. Qi, D. Gao, L. Zhang, and Y. Yang, Appl. Surf. Sci. **256**, 2507 (2010).
[45]B. K. Meyer, H. Alves, D. M. Hofmann, W. Kriegseis, D. Forster, F. Bertram, J. Christen, A. Hoffmann, M. Straßburg, M. Dworzak, U. Haboeck, and A. V. Rodina, Phys. Status Solidi B **241**, 231 (2004).
[46]Ü. Özgür, Y. I. Alivov, C. Liu, A. Teke, M. A. Reshchikov, S. Dogan, V. Avrutin, S. J. Cho, and H. Morkoc, J. Appl. Phys. **98**, 041301 (2005).
[47]D. C. Look, G. C. Farlow, P. Reunchan, S. Limpijumnong, S. B. Zhang, and K. Nordlund, Phys. Rev. Lett. **95**, 225502 (2005).
[48]Y. Liu, H. Liang, L. Xu, J. Zhao, J. Bian, Y. Luo,Y. Liu, W. Li, G. Wu, and G. Du, J. Appl. Phys. **108**, 113507 (2010).
[49]R. Dingle, Phys. Rev. Lett. **23**, 579 (1969).
[50]H. J. Xu, H. C. Zhu, X. D. Shan, Y. X. Liu, J. Y. Gao, X. Z. Zhang, J. M. Zhang, P. W. Wang, Y. M. Hou, and D. P. Yu, J. Phys.: Condens. Matter **22**, 016002 (2010).
[51]J. Goldberger, D. J. Sirbuly, M. Law, and P. Yang, J. Phys. Chem. B **109**, 9 (2005).
[52]K. Potzger and S. Zhou, Phys. Status Solidi B **246**, 1147 (2009).
[53]A. Ney, K. Ollefs, S. Ye, T. Kammermeier, V. Ney, T. C. Kaspar, S. A. Chambers, F. Wilhelm, and A. Rogalev, Phys. Rev. Lett. **100**, 157201 (2008).
[54]T. C. Droubay, D. J. Keavney, T. C. Kaspar, S. M. Heald, C. M. Wang, C. A. Johnson, K. M. Whitaker, D. R. Gamelin, and S. A. Chambers, Phys. Rev. B **79**, 155203 (2009).
[55]A. Barla, G. Schmerber, E. Beaurepaire, A. Dinia, H. Bieber, S. Colis, F. Scheurer, J.-P. Kappler, P. Imperia, F. Nolting, F. Wilhelm, A. Rogalev, D. Müller, and J. J. Grob, Phys. Rev. B **76**, 125201 (2007).
[56]T. Tietze, M. Gacic, G. Schütz, G. Jakob, S. Brück, and E. Goering, New J. Phys. **10**, 055009 (2008).
[57]S. Kumar, B. H. Koo, C. G. Lee, S. Gautam, K. H. Chae, S. K. Sharma, and M. Knobel, Funct. Mater. Lett. **4**, 17 (2011).
[58]J. M. D. Coey, Solid State Sci. **7**, 660 (2005).
[59]M. S. Park and B. I. Min, Phys. Rev. B **68**, 224436 (2003).
[60]C.-R. Cho, J.-Y. Hwang, J.-P. Kim, S.-Y. Jeong, M.-S. Jang, W.-J. Lee, and D.-H. Kim, Jpn. J. Appl. Phys. **43**, L1383 (2004).
[61]K. Samanta, P. Bhattacharya, and R. S. Katiyar, J. Appl. Phys. **105**, 113929 (2009).
[62]M. H. F. Sluiter, Y. Kawazoe, P. Sharma, A. Inoue, A. R. Raju, C. Rout, and U. V. Waghmare, Phys. Rev. Lett. **94**, 187204 (2005).
[63]L. W. Guo, D. L. Peng, H. Makino, K. Inaba, H. J. Ko, K. Sumiyama, and T. Yao, J. Magn. Magn. Mater. **213**, 321 (2000).
[64]J. M. D. Coey, M. Venkatesan, and C. B. Fitzgerald, Nature Mater. **4**, 173 (2005).
[65]H. S. Hsu, J. C. A. Huang, Y. H. Huang, Y. F. Liao, M. Z. Lin, C. H. Lee, J. F. Lee, S. F. Chen, L. Y. Lai, and C. P. Liu, Appl. Phys. Lett. **88**, 242507 (2006).
[66]H. Liu, X. Zhang, L. Li, Y. X. Wang, K. H. Gao, Z. Q. Li, R. K. Zheng, S. P. Ringer, B. Zhang, and X. X. Zhang, Appl. Phys. Lett. **91**, 072511 (2007).
[67]Y. Liu, J. Yang, Q. Guan, L. Yang, Y. Zhang, Y. Wang, B. Feng, J. Cao, X. Liu, Y. Yang, and M. Wei, J. Alloy. Compd. **486**, 835 (2009).
[68]V. B. Kopylov and E. V. Sergeev, Russ. J. Gen. Chem. **78**, 1111 (2008).
[69]M. Wei, N. Braddon, D. Zhi, P. A. Midgley, S. K. Chen, M. G. Blamire, and J. L. MacManus-Driscoll, Appl. Phys. Lett. **86**, 72514 (2005).
[70]G. Weyer, H. P. Gunnlaugsson, R. Mantovan, M. Fanciulli, D. Naidoo, K. Bharuth-Ram, and T. Agne, J. Appl. Phys. **102**, 113915 (2007).
[71]S. Yılmaz, M. Parlak, Ş. Özcan, M. Altunbaş, E. McGlynn, and E. Bacaksız, Appl. Surf. Sci. **257**, 9293 (2011).